Reports

Global Trends in Total Ozone

Kenneth P. Bowman

Satellite ozone data from the Total Ozone Mapping Spectrometer from 1979 through 1986 show that recent decreases of total ozone have not been confined to the Antarctic spring season (the Antarctic ozone hole), but are global in extent. The losses are about twice the estimated uncertainty in the satellite data. The decreases are largest in middle and high latitudes and occur in all seasons of the year. The decreases for this 8-year period are comparable in magnitude to the increases observed during the 1960s. Southern Hemisphere values from 1986 are generally greater than those from 1985.

During the last decade, total column ozone amounts over Antarctica in the springtime (September through November) have decreased by 30 to 40%, a phenomenon known as the Antarctic ozone hole. The decrease was first discovered in observations made with Dobson spectrophotometers on the ground (*1*) and later confirmed by satellite observations (*2*). The ozone loss seems to begin in early to mid-September at the end of the polar night. Unfortunately, few observations are available from the winter season. The area of unusually low ozone values reaches a maximum in mid-October to early November and disappears toward the end of November when the atmospheric circulation over Antarctica completes its transition to summertime patterns (*3*). Low ozone values are typical of the Antarctic in the springtime and have been observed since the International Geophysical Year (*1*, *4*), but the total ozone amounts observed in recent years are much lower than long-term averages, and are probably the lowest values ever recorded anywhere on Earth (*5*).

The distribution of ozone in the atmosphere is controlled by photochemical processes and the atmospheric circulation. Models of stratospheric ozone predict that man-made chemicals such as chlorofluorocarbons (CFCs) will cause significant losses of total ozone in coming decades if production and release into the atmosphere continue at present levels (*6*). Detecting the effects of man-made chemicals is difficult, because ozone also fluctuates from natural causes, such as variations in the atmospheric circulation. The rapid drop in Antarctic ozone, however, was not predicted by earlier models or expected from natural variability. Current theories suggest that the ozone hole is not the result of standard ozone photochemistry, but instead is due to man-made chemicals and previously unknown reaction processes associated with the cold Antarctic stratosphere (*7*). Although circulation effects have not been entirely ruled out (*8*), the Antarctic ozone hole may be an early warning of future global ozone losses. Newly available satellite ozone observations discussed below now show that substantial losses of ozone have not been confined to the Antarctic springtime, but are global in extent.

The data used consist of 8 years (1979 to 1986) of total ozone measurements from the Total Ozone Mapping Spectrometer (TOMS) on the Nimbus 7 satellite (*9*). The TOMS uses backscattered solar ultraviolet radiation to produce daily maps of vertically integrated ozone (total ozone) over the entire sunlit portion of the globe. Nimbus 7 is in a noon-midnight near-polar orbit, so that observations are made near local noon at all locations. Since sunlight is required, no measurements can be made within the polar night. Power limitations and various problems caused the loss of about 60 days of data during the first 9 months of operation, but few data are missing after June 1979.

The spatial resolution of the TOMS sensor varies from $\sim$50 to $\sim$250 km and depends on the viewing angle. The high-resolution scanner data were area-averaged onto a 5° by 5° latitude-longitude grid as described in Bowman and Krueger (*10*). All of the data used were completely reprocessed with the most recent version of the retrieval algorithm (*11*), which uses the new measurements of the ozone absorption cross section (*12*).

The root-mean-square precision of the TOMS ozone retrievals with respect to the ground-based Dobson network is $\sim$2% (*13*), but the calibration of the TOMS instrument remains a concern. The Solar Backscatter Ultraviolet (SBUV) instrument (a companion to the TOMS) has been compared to the Dobson network. During the period 1979 to 1984, the SBUV decreased relative to the Dobson network at 0.38 ± 0.13% per year (*11*). At the present time it is not known whether the increasing bias is caused by uncorrected drift in the SBUV, global increases in tropospheric ozone (which would affect the Dobson network more strongly), or local increases in ozone around the Dobson stations from urbanization. The SBUV drift does not appear to depend on latitude, whereas the trends in the TOMS data shown below are strongly latitude-dependent. This suggests that although the absolute trends may be uncertain, local trends in total ozone are significant. Drift in the TOMS instrument should be similar to that of the SBUV, since they share some internal calibration components, but a detailed intercomparison with the Dobson network is needed for verification. Except where specifically mentioned, results presented below are not corrected relative to the Dobson network. Future improvements to the TOMS calibration could be applied directly to the area-averaged results presented here.

The daily global mean total ozone for the 8-year period is plotted in Fig. 1. About 75 days were omitted from a total of 2922, because observations were available from less than 50% of the globe on those days. The annual cycle that appears in the global mean is the result of a larger annual cycle in

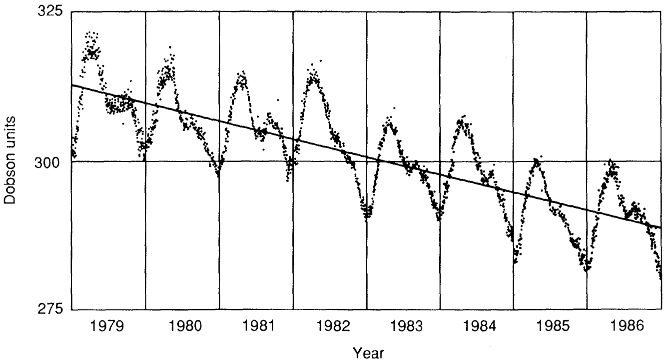

Fig. 1. TOMS daily global mean total ozone in Dobson units (1 Dobson unit = 10^{-3} atm cm) for 1979 to 1986. Each dot represents the global mean for 1 day. The time mean for the period is 301.1 Dobson units. The straight line is a least-squares fit to the data and has a slope of −1.0% per year.

Department of Atmospheric Sciences, University of Illinois at Urbana-Champaign, Urbana, IL 61801.

the Northern Hemisphere than in the Southern Hemisphere. The trend in the global mean total ozone as estimated by a least-squares fit to a straight line is −1.0% per year (as a percentage of the time mean value). The decrease is not confined to any individual season, as would be expected if the decrease in the global mean was the result of changes only in the Antarctic spring, but ranges from −0.9% for June-July-August to −1.1% for December-January-February. If the estimate of the instrument drift is correct, the decrease in global-mean total ozone during the 8-year period is ~5%.

The ozone losses show a strong latitude dependence but a weak seasonal dependence (Fig. 2; note that no trends can be computed in high-latitude winters because of the polar night). In the tropics the trend is nearly independent of season and ranges between about −0.5 and −1% per year. The losses generally increase with latitude outside the tropics and reach maxima at the poles. The loss rates are notably asymmetric about the equator, with considerably larger losses in the Southern than in the Northern Hemisphere, which probably reflects differences in the atmospheric circulations of the two hemispheres. The largest losses of about −4% per year occur in the Southern Hemisphere spring season. However, time mean ozone amounts are smaller in the Southern Hemisphere (*10*), so absolute changes, although still larger than those in the Northern Hemisphere, are not as large as percentage changes would indicate. Losses in the tropics would be near zero if allowances were made for the estimated instrumental drift, whereas losses in middle and high latitudes would still be substantial.

The local ozone trends are nearly zonally symmetric except in high latitudes and thus are not as geographically variable as London and Oltmans (*14*) reported for the period from 1961 to 1970. They reported increases on the order of 1% per year over most of the globe during that period. However, Bowman and Krueger (*10*) showed that global analyses from the Dobson network have substantial errors in data-sparse regions, which include the oceans and most of the Southern Hemisphere. London and Oltmans specifically noted that the negative trends they found over the Indian and South Pacific oceans were the result of their methods of analysis. From this one can surmise that trends in ozone during the 1960s were positive everywhere over the globe and reached maximum values of greater than 1% per year at high latitudes. The largest local decreases during the 1979 to 1986 period (of greater than 2% per year) occurred over East Antarctica and north of Scandinavia.

The TOMS data from 1986 indicate that ozone levels may be beginning to recover. Figure 3 shows daily zonal mean total ozone anomalies for the latitude band from 70° to 75°S. This latitude band is fairly representative of the Antarctic region as a whole, and since the polar night is brief at that latitude, data are available for almost the entire year. The time mean total ozone for the 8-year period at this latitude is 302.5 Dobson units (1 Dobson unit = 10^{-3} atm cm). Anomalies were computed by subtracting the climatological ozone value for each day, defined as the average for the 8 years for that calendar day, from the daily values. This transformation removes the climatological annual cycle, which is nearly sawtooth shaped at this latitude (*10*). The spikes in the time series are caused by year-to-year variations in the timing of the breakdown of the polar vortex, which is responsible for the sawtooth shape of the annual cycle, with respect to the climatological annual cycle (*3*). Zonal mean ozone amounts during the second half of 1986 are comparable to values from 1984 and considerably higher than those of 1985. Global mean ozone anomaly values for 1986 are also generally higher than during equivalent seasons in 1985 and indicate that the increase also is not restricted to the Antarctic. Garcia and Solomon (*15*) suggested that there is a quasi-biennial oscillation (QBO) signal superimposed on the downward trend. They attribute the 1986 increase to the QBO and predict that 1987 total ozone values will continue downward. If the TOMS continues to function, this hypothesis should be tested soon.

The TOMS data can be compared to recent analyses of observations from the Dobson network. The trends in the TOMS data reported here are much larger than those in the Dobson data presented by Angell (*16*) for the period from 1975 to 1984. This probably results from the different time periods used in the two analyses. Global total ozone reached high levels in 1978 and 1979 (at the time Nimbus 7 was launched) and have declined since then. Thus total ozone reached a peak in the middle of their analysis period but a maximum at the beginning of the TOMS data set. Rood (*17*) noted that global total ozone levels at the present time are comparable to the minimum levels reached in the early 1960s. Global ozone increased during the 1960s, as discussed above, so the recent decrease is not unprecedented.

The global extent of the ozone losses implies that the decrease is not due solely to local processes in the Antarctic, but it does not distinguish between chemical and dynamical, or natural and human loss mechanisms. The ozone decreases observed in the TOMS data are of comparable magnitude to increases observed with the Dobson network in the 1960s and 1970s. This suggests that the recent losses may be natural and

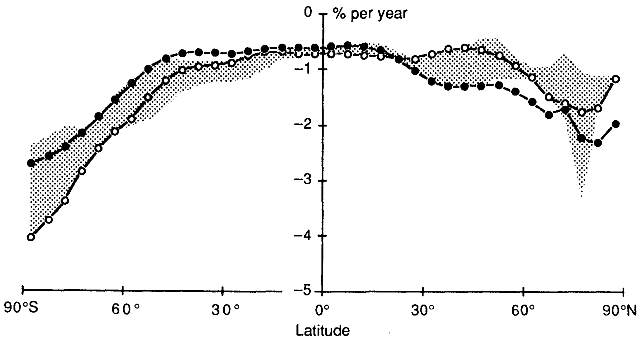

Fig. 2. Trends in zonal mean total ozone for the years 1979 to 1986. The solid dots represent trends in all of the available data at each latitude. The white dots are the trends in data from the September-October-November (Southern Hemisphere spring) period only. The shading indicates the range of trends (minimum and maximum) for the four individual seasons. Seasonal differences in the trends are relatively small in the tropics and larger in the polar regions.

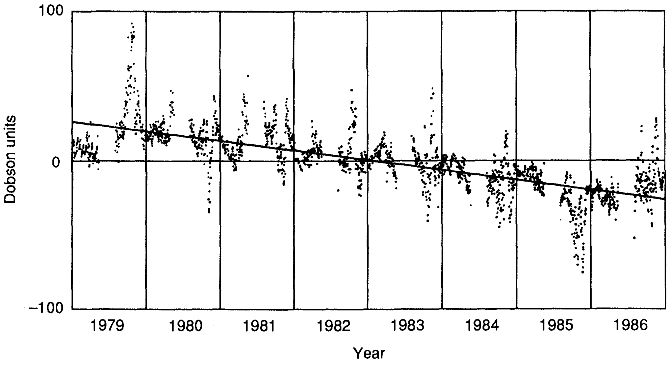

Fig. 3. Daily zonal mean total ozone anomalies for the latitude band from 70° to 75°S. Each dot represents the zonal mean anomaly for 1 day. Gaps in the time series are due to the polar night. The straight line is a least-squares fit to the data; it has a slope of −2.1% per year.

may result from long-term fluctuations of the general circulation of the stratosphere, such as a decrease in the strength of the Brewer-Dobson circulation. However, measurements of the stratospheric circulation are sparse, and inferring the transport of photochemically active trace species is difficult. The Upper Atmosphere Research Satellite (scheduled to be launched in the early 1990s) should improve our understanding of the stratospheric circulation and allow a better evaluation of the relative importance of the various loss mechanisms.

REFERENCES AND NOTES

1. J. C. Farman, B. G. Gardiner, J. D. Shanklin, *Nature (London)* **315**, 207 (1985).
2. R. S. Stolarski *et al.*, *ibid.* **322**, 808 (1986).
3. K. P. Bowman, *Geophys. Res. Lett.* **13**, 1193 (1986).
4. G. M. B. Dobson, *Q. J. R. Meteorol. Soc.* **92**, 549 (1966).
5. Most of the available data on the ozone hole, including observations of ozone, other trace species, and the atmospheric circulation, were presented in a special issue of *Geophysical Research Letters* [vol. 13, no. 12 (1986)].
6. National Research Council, *Halocarbons: Effects on Stratospheric Ozone* (National Academy of Sciences, Washington, DC, 1976); *Stratospheric Ozone Depletion by Halocarbons: Chemistry and Transport* (National Academy of Sciences, Washington, DC, 1979); *Causes and Effects of Stratospheric Ozone Reduction: An Update* (National Academy of Sciences, Washington, DC, 1982); "Atmospheric Ozone," *World Meteorol. Organ. Rep. No. 16* (World Meteorological Organization, Geneva, 1985).
7. S. Solomon, R. R. Garcia, F. S. Rowland, D. J. Wuebbles, *Nature (London)* **321**, 755 (1986); M. B. McElroy, R. J. Salawitch, S. C. Wofsy, J. A. Logan, *ibid.*, p. 759.
8. K.-K. Tung, M. K. W. Ko, J. M. Rodriguez, N. D. Sze, *ibid.* **322**, 811 (1986); J. D. Mahlman and S. B. Fels, *Geophys. Res. Lett.* **13**, 1316 (1986).
9. TOMS ozone data are processed by the Ozone Processing Team at NASA Goddard Space Flight Center (GSFC) under the direction of D. Heath. Data are available from the National Space Science Data Center at GSFC.
10. K. P. Bowman and A. J. Krueger, *J. Geophys. Res.* **90**, 7967 (1985).
11. A. J. Fleig *et al.*, *Geophys. Res. Lett.* **13**, 1355 (1986); A. J. Fleig, P. K. Bhartia, D. S. Silberstein, *ibid.*, p. 1359.
12. A. M. Bass and R. J. Paur, in *Atmospheric Ozone, Proceedings of the Quadrennial Ozone Symposium, 1984*, C. S. Zerefos and A. Ghazi, Eds. (Reidel, Dordrecht, 1985), p. 611.
13. P. K. Bhartia, K. F. Klenk, C. K. Wong, D. Gordon, *J. Geophys. Res.* **89**, 5239 (1984).
14. J. London and S. J. Oltmans, *Pure Appl. Geophys.* **117**, 345 (1978).
15. R. R. Garcia and S. Solomon, *Geophys. Res. Lett.* **14**, 848 (1987).
16. J. K. Angell, *Mon. Weather Rev.* **115**, 753 (1987).
17. R. B. Rood, *Geophys. Res. Lett.* **13**, 1244 (1986).

18. This work was supported by the NASA Upper Atmosphere Theory and Data Analysis Program through grant NAGW-992 to the University of Illinois at Urbana-Champaign.

21 August 1987; accepted 17 November 1987

Atomic Force Microscopy of an Organic Monolayer

O. Marti, H. O. Ribi, B. Drake, T. R. Albrecht, C. F. Quate,
P. K. Hansma

Atomic force microscope images of polymerized monolayers of *n*-(2-aminoethyl)-10,12-tricosadiynamide revealed parallel rows of molecules with a side-by-side spacing of ≈0.5 nanometer. Forces used for imaging (10^{-8} newton) had no observable effect on the polymer strands. These results demonstrate that atomic force microscope images can be obtained for an organic system.

The atomic force microscope (AFM) (*1–5*) is a new instrument suitable for imaging surfaces. The images consist of a series of parallel profiles of a surface. Each profile is obtained by moving a tip, which ideally is terminated by a single atom, across the surface with a small tracking force on the order of 10^{-8} N. Predecessors of this instrument include profilometers (*6–8*), the topografiner (*9*), and scanning tunneling microscopes (STM) (*10, 11*). The AFM, unlike the STM, is not restricted to conductive or semiconductive surfaces. Atomic resolution imaging (*2, 4*) that approaches the resolving power of STMs and is much better than that of stylus profilometers has been demonstrated with AFMs. We report AFM images of organic molecules.

Our AFM design is an extension of an earlier STM design (*12*) and an improved version of the first operational AFM design (*4*) by our group. As shown in Fig. 1, the sample is mounted on an (*x,y,z*) scanner (*13*) and pressed against a diamond tip mounted on a triangular microcantilever (*5*) with a spring constant of ≈1 N/m. The deflection of the microcantilever is monitored by sensing the tunneling current between the back of the microcantilever and a platinum-iridium point. Deflections for the data reported were on the order of 10 nm, which resulted in forces between the tip and the sample on the order of 10^{-8} N. During imaging the deflection was kept constant by a feedback loop that controlled the height *z* of the sample.

The dominant mass of the microcantilever–diamond tip assembly in our microscope is the mass of the diamond tip ($\approx 1 \times 10^{-10}$ kg). This mass and the spring constant of the cantilever together give a resonant frequency of ≈16 kHz, which is in agreement with the performance of the microscope. The repulsive interaction with the surface creates another spring in parallel to the cantilever and increases the overall resonant frequency during operation.

We imaged polymerized monolayers of AE-TDA [*n*-(2-aminoethyl)-10,12-tricosadiynamide] because this compound is well defined chemically and films in the polymerized state show a high degree of structural integrity when transferred to glass supports. This compound was prepared as the polymerizable surfactant by attaching ethylenediamine through the amide linkage to 10,12-tricosadiynoic acid.

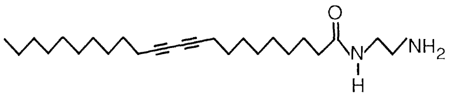

1

Monolayers of AE-TDA were formed at the air-water interface by standard methods (*14*). The films were compressed to near their collapse pressure (~0.05 N/m) to ensure that they were in a crystalline state, and they were then polymerized by ultraviolet irradiation. The films had a pink-blue appearance indicative of the conjugated polydiacetylene polymer (*15*). After polymerization, the monolayers were transferred to glass chips with the hydrophilic side of the film abutting to the surface of the glass. Attachment of the monolayers to the glass surface was confirmed by fluorescent microscopy. The polymer layers appeared bright orange-red under magnifications of ×40 to ×200 when the light was filtered with a rhodamine filter. The monolayers were comprised of tightly packed microcrystalline domains between 1 and 100 μm in diameter and covered a total surface area of 70 to 80%. Domains similar in dimension and distribution were observed by transmission electron microscopy when the polymerized monolayers were transferred to nitrocellulose-coated microscope grids (*16*).

O. Marti, B. Drake, P. K. Hansma, Department of Physics, University of California, Santa Barbara, CA 93106.

H. O. Ribi, Department of Cell Biology, Stanford University, Stanford, CA 94305.

T. R. Albrecht and C. F. Quate, Edward L. Ginzton Laboratory, W. W. Hansen Laboratories of Physics, Stanford University, Stanford, CA 94305.